Internal reconnection for northward interplanetary magnetic field

Masakazu Watanabe,[1] Konstantin Kabin,[2] George J. Sofko,[1] Robert Rankin,[2]
Tamas I. Gombosi,[3] Aaron J. Ridley,[3] and C. Robert Clauer[3]

Received 7 October 2004; revised 23 January 2005; accepted 8 March 2005; published 24 June 2005.

[1] On the basis of magnetohydrodynamic simulation results for northward interplanetary magnetic field (IMF) and significant dipole tilt, we describe internal reconnection processes that occur earthward of the magnetopause subsequent to magnetopause reconnection. We discuss the associated ionospheric signatures and show that the internal reconnection occurs not only between a summer lobe and a winter lobe field line but also between a summer lobe field line and a closed field line. The latter internal reconnection drives a pair of convection cells circulating outside the polar cap in the winter ionosphere. In this paper, we refer to these convection cells as "reciprocal cells" and the corresponding reconnection as reciprocal cell reconnection. The reciprocal cells are coupled to the so-called lobe cells that are driven by magnetopause reconnection between an IMF line and a summer lobe field line (lobe cell reconnection); these lobe cells circulate inside the polar cap in the summer ionosphere. The reciprocal cell reconnection converts an overdraped lobe field line to a relaxed lobe field line, while the lobe cell reconnection converts a relaxed lobe field line to an overdraped lobe field line. Thus the reciprocal cell reconnection reciprocates with the lobe cell reconnection through the exchange of magnetic flux.

Citation: Watanabe, M., K. Kabin, G. J. Sofko, R. Rankin, T. I. Gombosi, A. J. Ridley, and C. R. Clauer (2005), Internal reconnection for northward interplanetary magnetic field, *J. Geophys. Res.*, *110*, A06210, doi:10.1029/2004JA010832.

1. Introduction

[2] The process of internal reconnection for northward interplanetary magnetic field (IMF) was first introduced by *Crooker* [1992] following the concept of sequential reconnection by *Cowley* [1983]. Figure 1 depicts four types of magnetic reconnection that are physically possible for due northward IMF and significant dipole tilt. In each figure, the left side shows field lines before the reconnection, and the right side shows field lines after the reconnection. We have assumed boreal summer, with all figures viewed from dusk, with the Sun on the left. Reconnection occurs at the cross marked on each figure. Figure 1a shows the initial reconnection between an incoming IMF line and a closed geomagnetic field line on the magnetopause in the summer hemisphere. As a result, two open field lines are created. One of these is connected to the summer ionosphere (summer lobe) and overdrapes the dayside magnetosphere, while the other is connected to the winter ionosphere (winter lobe) and overdrapes the nightside magnetosphere. Figure 1b shows the subsequent reconnection between the two lobe field lines in the magnetospheric boundary region in the winter hemisphere. The magnetic flux returns to the closed region by this reconnection. This second stage of reconnection was called internal reconnection by *Crooker* [1992] because it occurs inside the magnetopause.

[3] Recently, another type of internal reconnection has been postulated by *Watanabe et al.* [2004]. They interpreted the simulation results by *Tanaka* [1999], for northward IMF with the clock angle of 45° (no dipole tilt), in terms of sequential reconnection that causes polar cap bifurcation in the polar ionosphere. *Watanabe et al.* [2004] also showed observational evidence that supports their idea. In their model, an IMF line approaching the Earth first reconnects with a closed geomagnetic field line on the high-latitude magnetopause in one hemisphere. This reconnection produces a normal lobe field line connected to the ionosphere in the same hemisphere as the reconnection point and an overdraped lobe field line connected to the ionosphere in the opposite hemisphere (the geometry of this reconnection is somewhat different from Figure 1a; see Figure 1 of *Watanabe et al.* [2004]). Subsequently, the overdraped lobe field line reconnects with a closed field line within the magnetospheric boundary layer in the same hemisphere as the magnetopause reconnection point, converting the overdraped lobe field line to a normal lobe field line. The topology of this reconnection is shown in Figure 1d. *Watanabe et al.* [2004] called the second reconnection internal reconnection following *Crooker* [1992]. However, from the point of view of magnetic flux transport, the *Watanabe et al.* [2004] type internal reconnection

[1]Department of Physics and Engineering Physics, University of Saskatchewan, Saskatoon, Saskatchewan, Canada.
[2]Department of Physics, University of Alberta, Edmonton, Alberta, Canada.
[3]Department of Atmospheric, Oceanic, and Space Sciences, University of Michigan, Ann Arbor, Michigan, USA.

0148-0227/05/2004JA010832

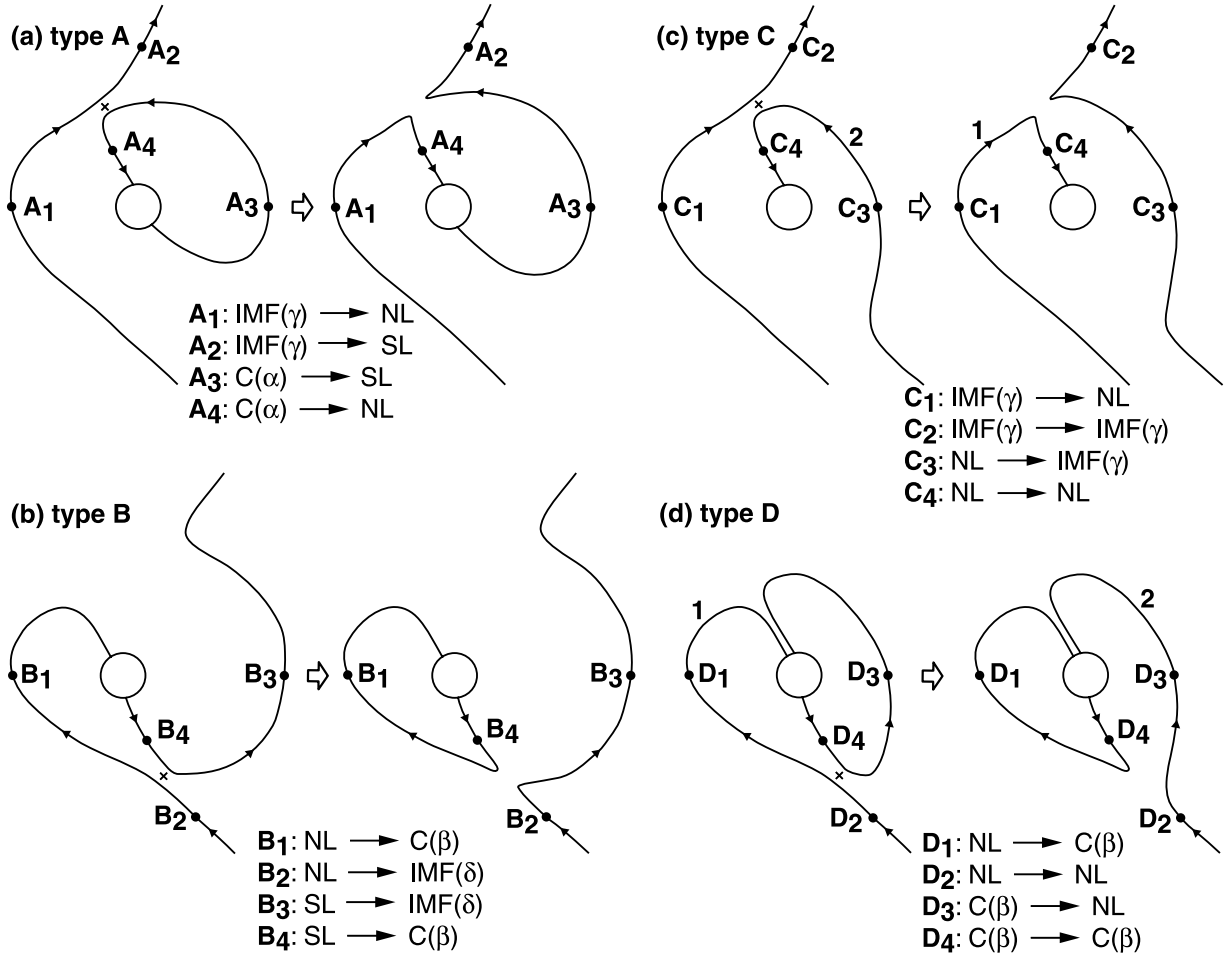

Figure 1. Schematics representing the change of magnetic topology during the four types of reconnection. All figures are views from the duskside, and the Sun is to the left. Magnetic field lines are not necessarily in the noon-midnight meridian plane. Crosses show the reconnection points. For each type of reconnection, four kinds of topological region transition (see section 5) are identified: A_1 to A_4 for type A, B_1 to B_4 for type B, C_1 to C_4 for type C, and D_1 to D_4 for type D. Abbreviations of topological regions: IMF (Interplanetary Magnetic Field), C (Closed), NL (North Lobe), and SL (South Lobe).

(Figure 1d) for oblique northward IMF plays a different role from the *Crooker* [1992] type internal reconnection (Figure 1b) for purely northward IMF. While the latter completes the return of open magnetic flux to the closed region, the former enables the tailward transport of open magnetic flux by canceling the overdraping.

[4] *Watanabe et al.* [2004] suggested that their magnetic flux circulation was incompatible with that of *Crooker* [1992]. Our present study was partly motivated by an effort to seek a unifying relationship between the two types of magnetic flux transport. Since *Crooker*'s [1992] model employs a simple superposition of magnetic fields in a vacuum, it is naturally limited to qualitative aspects of magnetospheric configuration. In the present work, we extend the original Crooker model by performing a high-resolution magnetohydrodynamic (MHD) simulation of the Earth's magnetosphere for large dipole tilt under purely northward IMF conditions. As a result, some new aspects are revealed that were not available in the original Crooker model. One new feature is that the internal reconnection between an overdraped (summer lobe) field line and a closed field line (Figure 1d) also occurs for a due northward IMF and a tilted dipole. In addition, this internal reconnection is coupled to the magnetopause reconnection between an IMF line and an open geomagnetic (summer lobe) field line in the opposite hemisphere (Figure 1c). The purpose of this paper is to describe this new internal reconnection process and its ionospheric signatures. We will return to Figure 1 later in the paper.

[5] Although this paper deals with magnetospheric processes, our main interest is in their ionospheric signatures. In fact, our main motivation for this work is experimental measurements of ionospheric convection. We are preparing a sequel to this paper that demonstrates observational evidence for our simulation results using Super Dual Auroral Radar Network (SuperDARN) data in conjunction with low-altitude satellite observations. To date, ionospheric convection is the only aspect of global magnetospheric dynamics which is amenable to direct observational verification. In situ satellite observations are somewhat limited for global dynamics studies because even multiple satellites cannot provide global information about the magnetosphere. Ionospheric convection for northward IMF and its related phenomena have been reported since the early

1970s. However, it was not until the late 1990s that truly two-dimensional observations of ionospheric convection became available through SuperDARN [e.g., *Huang et al.*, 2000]. As a diagnosis tool for magnetospheric studies, not only the convection pattern but also its relation to the open/closed field line boundary is important. For example, sunward convection for northward IMF occurs both on closed field lines and on open field lines; however, physical processes driving the convection are different for the two cases. Thus in this paper we emphasize ionospheric convection and its relation to the open/closed field line boundary, with a goal of providing a reference for interpreting ionospheric observations in future studies.

[6] As described previously, the theme of this paper is internal reconnection for northward IMF. Of course, our interpretation of the simulation results is based on the long history of modeling of magnetospheric merging configuration. There are two excellent reviews by *Siscoe* [1988] and *Crooker* [1990] on this subject, so we do not repeat a detailed review here. In this paper we refer to two canonical models. One is the null-separator model [*Dungey*, 1963; *Cowley*, 1973; *Stern*, 1973] obtained by superposing a dipole field and a uniform field. The other is the current penetration model [*Alekseyev and Belen'kaya*, 1983; *Crooker et al.*, 1990] which associates the merging process with a boundary current through which the magnetic field penetrates. The two models are not competing but complementary (see *Siscoe* [1988] and *Crooker* [1990] for details). A short description of these models will be given later when they are used in our discussion.

2. Model Description

[7] We use a magnetosphere-ionosphere coupling model recently developed at the University of Michigan. The mathematical basis for the description of the magnetosphere is provided by the equations of ideal single-fluid MHD. These equations are solved on a three-dimensional unstructured adaptive grid using an efficient Godunov-type finite volume method. The numerical details of this code are described by *Powell et al.* [1999], *DeZeeuw et al.* [2000], and references therein. Our simulation used about 4 million cells with the smallest cell being 1/12 R_E (R_E being the radius of the Earth). We did not include the effects of the Earth's rotation in our simulation. The coordinate system used in the model is the geocentric solar magnetospheric system: the X axis points from the Earth to the Sun, the Z axis is positive to the north and is in the plane containing the X axis and the Earth's dipole axis, and the Y axis completes the right-hand system. The ionosphere is represented by a two-dimensional layer with prescribed finite Pederson (Σ_P) and Hall (Σ_H) conductivities. Equations for the ionospheric potential are solved on a structured spherical grid with resolution of 1.4° in longitude and latitude. The magnetosphere-ionosphere coupling is performed as described in the works of *Goodman* [1995] and *Ridley et al.* [2004].

[8] In our simulation run, we used typical solar wind parameters: velocity V = 400 km/s, density N = 5 amu/cc, and temperature T = 50,000 K. Following *Crooker* [1992], we tilted the Earth's dipole axis 35° in the X-Z plane so that the northern hemisphere is in summer. This is the maximum dipole tilt at 1630 UT at the boreal summer solstice. The purely northward IMF was set to B_X = 0 nT, B_Y = 0 nT, and B_Z = 15 nT. For simplicity, we assumed uniform ionospheric conductivities: Σ_P = 2 S and Σ_H = 4 S for the northern (summer) ionosphere and Σ_P = 0.5 S and Σ_H = 1 S for the southern (winter) ionosphere. The discontinuity of the ionospheric conductance at the equator is not important because no magnetic fields map in the equatorial region. For these conditions, the simulation code was allowed to run until the system became quasi-stationary; the results presented are for this steady-state magnetosphere-ionosphere system.

3. Ionospheric Convection

[9] Figure 2 shows ionospheric potentials (i.e., streamlines) together with the open/closed field line boundary (we call it the polar cap boundary in this paper), in magnetic latitude (MLAT) and magnetic local time coordinates. We see twin reverse cells at high latitudes and a pair of crescent-shaped cells at lower latitudes for both hemispheres. The latter may be driven by magnetospheric viscosity, while the former are driven by magnetic reconnection as we describe below. In this paper we focus on the reconnection-driven twin reverse cells. At high latitudes, overall, the potential patterns are very similar between the two hemispheres; they show twin reverse cells with their centers slightly shifted sunward from the dawn-dusk median. However, there are significant differences in relation to the polar cap boundary. In the northern ionosphere, on the one hand, the polar cap is heart-shaped and lies mostly on the dayside of the dawn-dusk meridian. The center of the polar cap is located at ~84° MLAT in the noon meridian. This feature is consistent with *Crooker*'s [1992] analytic model (her Figure 3). In the southern ionosphere, on the other hand, the polar cap is an oval centered on the geomagnetic pole. For convenience of the description below, we divide the polar caps in both hemispheres into two parts by the line passing through the approximate center of the polar cap and parallel to the dawn-dusk line. We call the sunward half of the polar cap the "front half" of the polar cap and the other half of the polar cap the "back half" of the polar cap. This division is not exact. We use "front half" and "back half" to indicate approximate location with respect to the "center" of the polar cap. In the northern ionosphere, the location of the convection cells is shifted toward the back half, while in the southern ionosphere, it is shifted toward the front half. As a result, the fastest sunward flow occurs in the back half (front half) of the polar cap in the northern (southern) ionosphere. This interhemispheric asymmetry results from the topology of the magnetic field. As we show later on, field lines participating in reconnection in the northern (southern) hemisphere have their feet in the northern (southern) ionosphere near the back half (front half) of the polar cap boundary.

[10] The arrows in Figure 2 indicate the location of the electric potential maxima/minima on the polar cap boundary. An important interhemispheric difference is that the potential peaks (the centers of the convection cells) in the northern ionosphere are located poleward of the polar cap boundary, while in the southern ionosphere they are equatorward of the polar cap boundary. As a result, in the northern ionosphere there are small twin convection cells circulating within the polar cap, while in the southern

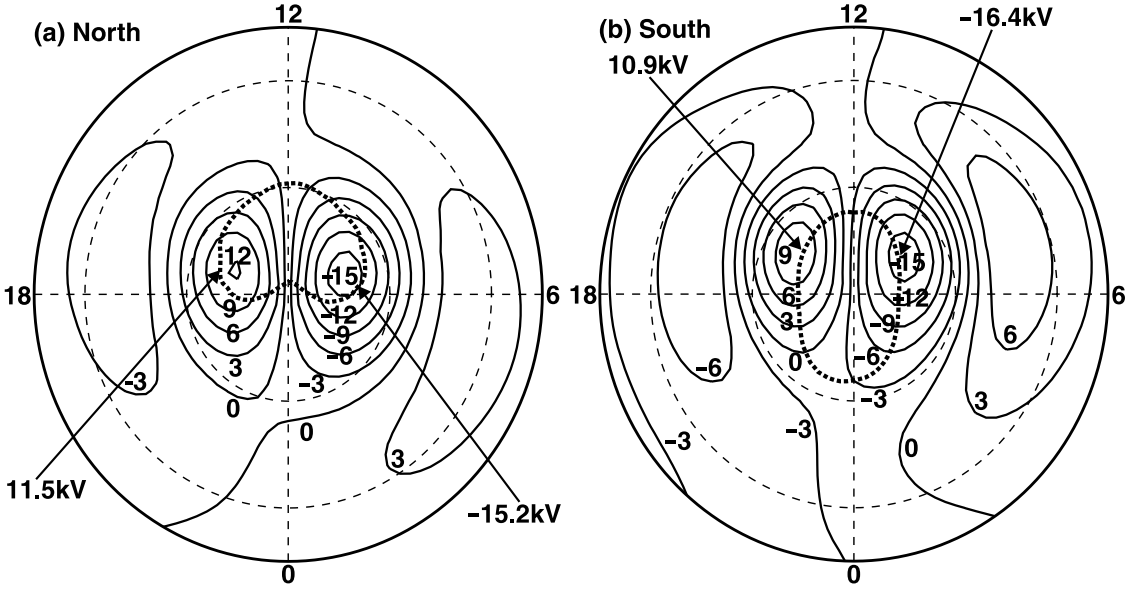

Figure 2. Ionospheric potential contours (solid lines) together with the open/closed field line boundary (thick dotted lines) (a) in the northern ionosphere and (b) in the southern ionosphere, in magnetic latitude (MLAT) and magnetic local time coordinates. The dashed concentric circles show 80° and 70° MLATs, and the outermost solid circle corresponds to 65° MLAT. Potential values are labeled in kV. The four arrows indicate the potential peaks on the open/closed field line boundary (the footpoints of ''droplines'').

ionosphere there are tiny twin convection cells circulating outside the polar cap. We call the former convection cells ''lobe cells,'' following the nomenclature by *Reiff and Burch* [1985]. On the other hand, we call the latter convection cells ''reciprocal cells,'' in the sense that they reciprocate with lobe cells. Formation mechanisms of reciprocal cells and their coupling to lobe cells are the main topics of this paper. The convection cells that intersect the polar cap boundary twice in one cycle are merging cells [*Reiff and Burch*, 1985], and it is within them that the lobe cells and the reciprocal cells are imbedded. All of the convection cells described above are driven by merging.

4. Magnetospheric Topology

[11] In order to investigate reconnection processes in the magnetosphere, we first need to know its topology. The magnetic topology in our simulation is basically the same as the superposed field model by *Dungey* [1963] and *Cowley* [1973]. In this section, we first summarize this superposition model and then apply it to our simulation results.

4.1. Vacuum Superposition Model (Null-Separator Model)

[12] When a dipole field and a uniform IMF are superposed in a vacuum, there appear three topological classes of magnetic field lines: (1) closed field lines (both ends are connected to the Earth) contained inside a volume topologically identical to a torus, (2) IMF lines (both ends are unconnected to the Earth) lying outside a volume topologically identical to a cylinder, and (3) open field lines (one end is connected to the Earth, but the other end is unconnected to the Earth) occupying the volume outside the torus but inside the cylinder. The surfaces of the torus and the cylinder are called separatrices. Each separatrix consists of a bunch of magnetic field lines diverging from or converging to a magnetic null.

[13] Figure 3 shows the separatrix surfaces of the vacuum superposition model (adapted from Figure 15 of *Siscoe* [1988], which derives from Figures 9–12 of *Cowley* [1973]). Field lines on the torus are shown by dotted lines. The surface of the torus touches the surface of the cylinder along a curve which is topologically equivalent to a circle and encompasses the Earth. The circle consists of two magnetic field lines, called separators, connecting two magnetic nulls (A and B in Figure 3) on the circle. In accordance with the null-point classification scheme of *Cowley* [1973], the two field lines diverge from null B and converge to null A. The surface of the torus above the separator circle (see Figure 3) is made up of all the field lines that diverge from null B and go into the northern ionosphere. These field lines form the polar cap boundary in the northern ionosphere. Similarly, the surface of the torus below the separator circle is made up of all the field lines from the southern ionosphere that converge to null A. These field lines form the polar cap boundary in the southern ionosphere. On the other hand, the surface of the cylinder above the separator circle (see Figure 3) is made up of all the field lines from infinity that converge to null A. Similarly, the surface of the cylinder below the separator circle is made up of all the field lines that diverge from null B and go to infinity. There are two singular field lines diverging from null A, one on the torus surface going to the northern ionosphere and the other on the cylinder surface going to infinity (see Figure 3). Similarly, there are two singular field lines converging to null B, one on the torus surface coming from the southern ionosphere and the other on the cylinder surface coming from infinity. The singular line connecting a null and the ionosphere was called the ''stemline'' by *Siscoe et al.* [2001]. In this paper we refer to

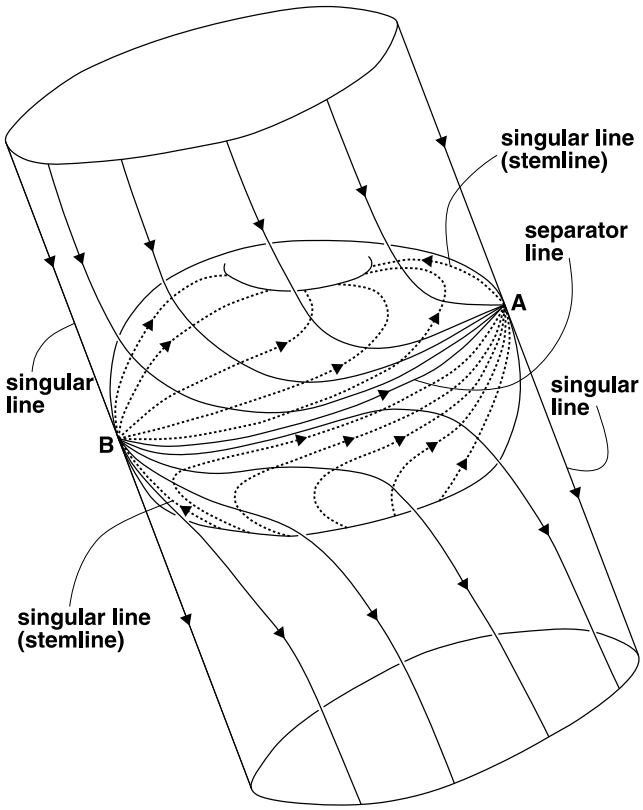

Figure 3. The separatrix surfaces (topologically a torus and a cylinder) resulting from superposition of a dipole field and a uniform field, with the arrowed lines representing magnetic field lines on the separatrix surfaces. Field lines on the torus surface are shown by dotted lines. (Adapted from Figure 15 of *Siscoe* [1988].)

the magnetospheric topology of Figure 3 proposed by *Dungey* [1963] and *Cowley* [1973] as the null-separator model.

4.2. Simulation Results

[14] Although the null-separator model makes no provision for magnetic fields from magnetopause currents and several other sources (see *Siscoe* [1988] and *Crooker* [1990]), recent simulations show that this vacuum model holds true even in the MHD context [*Crooker et al.*, 1998; *Siscoe et al.*, 2001]. Our simulation results also show that the null-separator model is a fairly good approximation. *Greene* [1988] argues that the null-separator topology is stable to magnetic field perturbations and cannot be destroyed easily by any physical process. Thus we adopt the null-separator topology in our MHD model. Practically, null points are relatively easy to find, while field lines connecting the nulls (separators) are difficult to find.

[15] Figure 4 shows, for our model magnetosphere (IMF $B_X = B_Y = 0$ and $B_Z = 15$ nT; dipole tilt = 35°), field lines traced from just equatorward of the duskside polar cap boundary in the southern ionosphere. In this paper we show only the duskside field lines. The dawnside field lines are basically a mirror image with respect to the noon-midnight meridian plane. The starting points of the tracing are shown in Figure 4d by solid circles. These points are virtually on the polar cap boundary in Figure 2b. All field lines from the southern polar cap boundary converge to a point in the northern hemisphere marked as M in Figure 4a and go into the northern ionosphere virtually as one singular field line (s_1). Point M is a magnetic null and corresponds to null A in Figure 3. The location of null M is (X, Y, Z) = (4.5, −0.2, 10.0) R_E with an accuracy of 1/12 R_E (the cell size in the vicinity of M). The footpoint of s_1 in the northern ionosphere is shown by an open circle in Figure 4d (it is actually superposition of many circles). The footpoint is located on the noon meridian and on the back half of the polar cap boundary in Figure 2a. Using a term coined by *Siscoe et al.* [2001], the singular line s_1 is one of the two stemlines.

[16] If we trace field lines from just poleward of the duskside polar cap boundary in the southern ionosphere, field lines take virtually the same paths as in Figures 4a–4c and converge to null M. Then all field lines go to infinity as one singular field line (s_3) shown by the dashed line in Figure 4a. Thus the surface defined by field lines in Figures 4a–4c is the nightside half of the torus in the null-separator model. In this paper we call this surface separatrix α.

[17] Figure 5 is similar to Figure 4 but shows field lines traced from just equatorward of the duskside polar cap boundary in the northern ionosphere. As in the previous case, all field lines from the northern polar cap boundary converge to a point in the southern hemisphere marked as N in Figure 5a and go into the southern ionosphere as one singular field line (s_2). Point N is the other magnetic null in the system and corresponds to null B in Figure 3. The location of null N is (X, Y, Z) = (−6.3, 0.3, −14.0) R_E with an accuracy of 1/3 R_E (the cell size in the vicinity of N). The line s_2 is the other stemline in the system. The footpoint of stemline s_2 in the southern ionosphere is shown by a solid circle in Figure 5d (which is again superposition of many circles). It is located on the noon meridian and on the front half of the polar cap boundary in Figure 2b.

[18] Similarly, if we trace field lines from just poleward of the duskside polar cap boundary in the northern ionosphere, field lines take virtually the same paths as in Figures 5a–5c and converge to null N. Then all field lines go to infinity as one singular field line (s_4) shown by the dashed line in Figure 5a. Thus the surface defined by field lines in Figures 5a–5c is the dayside half of the torus in the null-separator model. In this paper we call this surface separatrix β.

[19] Separatrix α (Figure 4) and separatrix β (Figure 5) form the torus in the null-separator model. Figure 6 is the combination of Figures 4 and 5 and represents a three-dimensional view of the duskside half of the torus. Blue lines show field lines representing separatrix α, and red lines show field lines representing separatrix β. In this view, the blue lines are behind the red lines when they intersect. Stemlines s_1 and s_2 are on the torus surface. There is a field line along which the red and blue lines in Figure 6 touch (the tangency line between separatrices α and β). This field line is the duskside separator which connects nulls N and M.

[20] We can determine the separatrices (cylinder) dividing the IMF and the open geomagnetic field in a similar manner. We first consider the southern half of the cylinder. By analogy with the polar cap (i.e., open/closed field line) boundary, we introduce the open/interplanetary field line

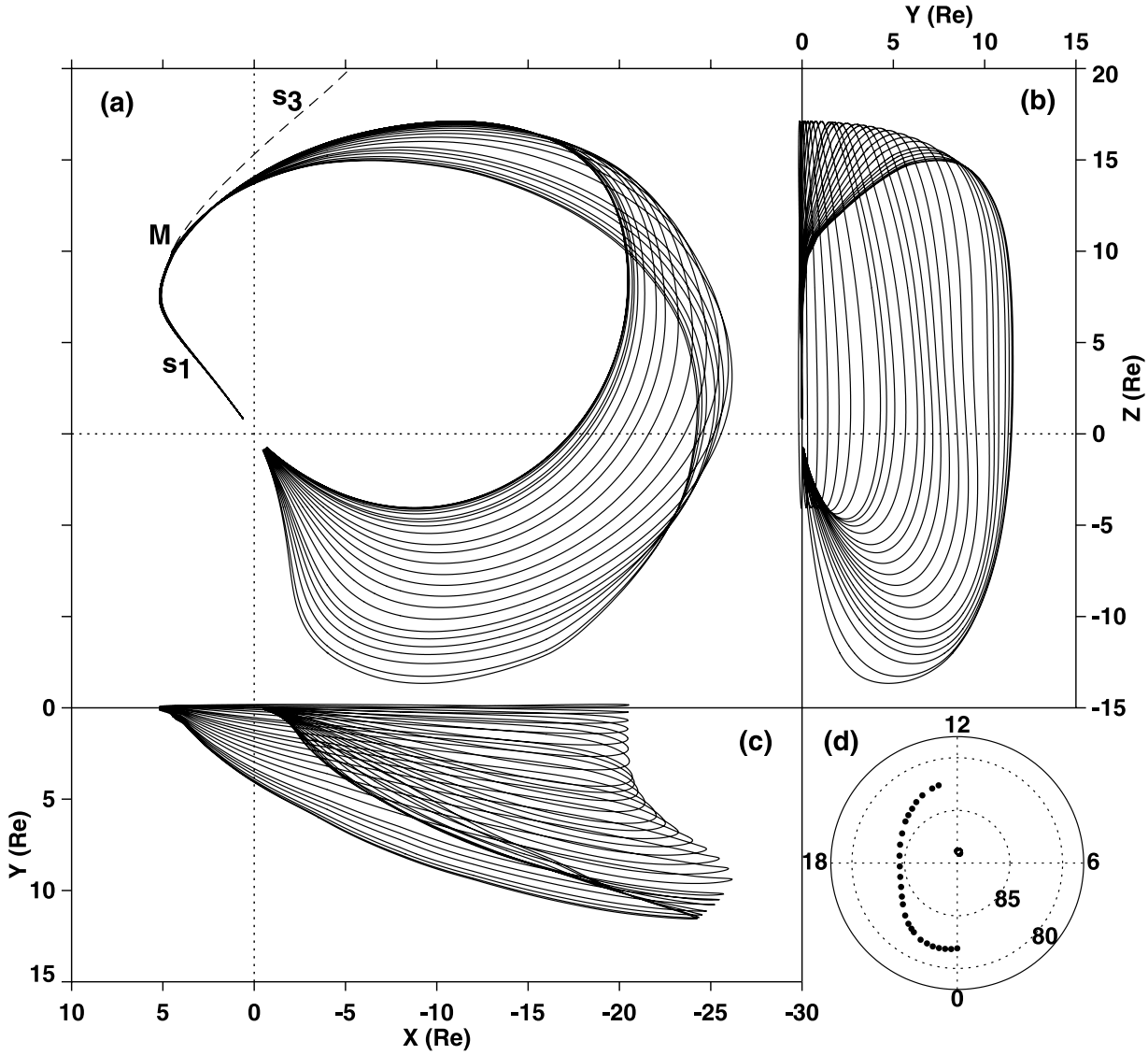

Figure 4. Field lines traced from just equatorward of the duskside polar cap boundary in the southern ionosphere: (a) projection onto the *X-Z* plane, (b) projection onto the *Y-Z* plane, and (c) projection onto the *X-Y* plane. Figure 4d shows the footpoints of the field lines in the northern ionosphere (open circles) and in the southern ionosphere (solid circles). The dashed line in Figure 4a shows a field line when the tracing is started from just poleward of the polar cap boundary in the southern hemisphere (see text for detail).

boundary in the plane $Z = -30\ R_E$. This reference plane is arbitrary, provided that it is far southward of null N. The boundary is a closed loop. Figure 7 shows field lines traced from just inside the duskside open/interplanetary field line boundary toward the Earth. Now all field lines converge to null M and go into the northern ionosphere virtually as one singular field line s_1 in Figure 7a, namely stemline s_1 in Figure 4a. The footpoint of stemline s_1 is shown by an open circle in Figure 7d. It is on the noon meridian and on the back half of the polar cap boundary in Figure 2a.

[21] If we trace field lines from just outside the duskside open/interplanetary field line boundary at $Z = -30\ R_E$, we obtain field lines very similar to Figures 7a–7c. All field lines converge to null M (they are virtually identical to Figures 7a–7c) and then go from null M to infinity as one singular field line shown by the dashed line s_3 in Figure 7a, namely the same singular line s_3 in Figure 4a. Thus the surface defined by field lines in Figures 7a–7c is the southern half of the cylinder in the null-separator model. In this paper we call this surface separatrix γ.

[22] Figure 8 shows the northern half of the cylinder determined in a similar manner. In this case, we define the open/interplanetary field line boundary in the plane $Z = +30\ R_E$. All field lines traced from just inside the duskside open/interplanetary field line boundary toward the Earth converge to null N and go into the southern ionosphere virtually as one singular field line (s_2 in Figure 8a, which is the same as s_2 in Figure 5a). Similarly, field lines from just outside the duskside open/interplanetary field line boundary converge to null N and then go to infinity as one singular

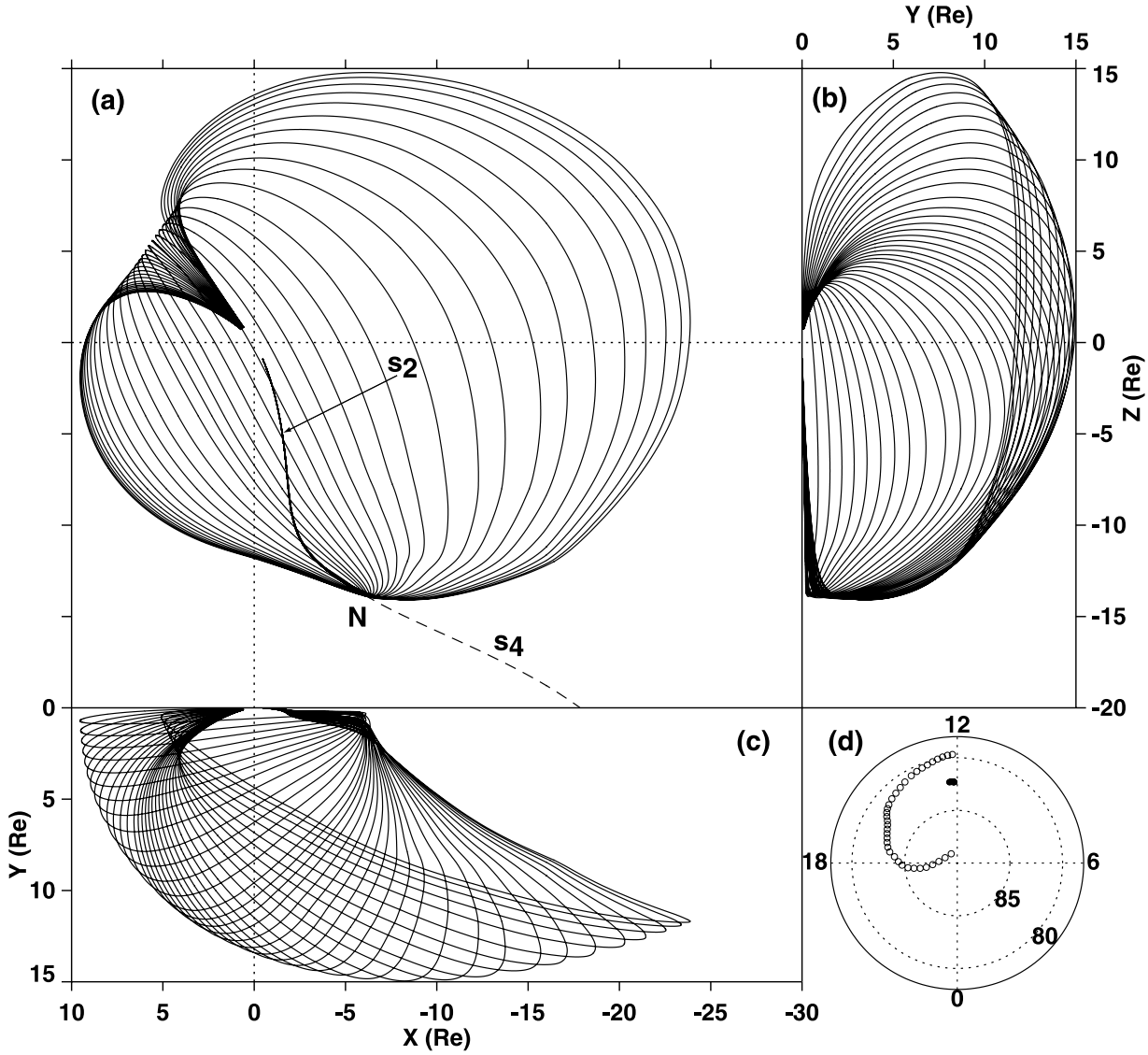

Figure 5. Field lines traced from just equatorward of the duskside polar cap boundary in the northern ionosphere, in the same format as Figure 4. The footpoints of the field lines are shown in Figure 5d by open circles (northern ionosphere) and solid circles (southern ionosphere). The dashed line Figure 5a is a field line when the tracing is started from just poleward of the polar cap boundary in the northern ionosphere.

field line s_4 (shown by the dashed line in Figure 8a, the same as s_4 in Figure 5a). Thus the surface defined by field lines in Figures 8a–8c is the northern half of the cylinder in the null-separator model. In this paper we call this surface separatrix δ.

[23] Separatrix γ (Figure 7) and separatrix δ (Figure 8) form the cylinder in the null-separator model. Figure 9 is the combination of Figures 7 and 8 and represents a three-dimensional view of the duskside half of the cylinder. Blue lines show field lines representing separatrix γ, and red lines show field lines representing separatrix δ. In this view, the blue lines are in front of the red lines when they intersect. Singular lines s_3 and s_4 are on the cylinder surface. There is a field line along which the red and blue lines in Figure 9 touch (the tangency line between separatrices γ and δ). This field line is the duskside separator described earlier.

5. Identifying Reconnection

[24] From the topology of the magnetic field only, we cannot know what kind of reconnection (or merging) is occurring. A reconnection process is identified by plasma flow crossing separatrices [e.g., *Vasyliunas*, 1975] or by a change of magnetic connectivity [e.g., *Axford*, 1984]. In section 4.1 we defined three topologically distinctive regions: (1) the closed region, (2) the IMF region, and (3) the open region. For identification of reconnection, we further divide each region into two subregions. First, we divide the closed region into the subregion facing separatrix α (Closed-α)

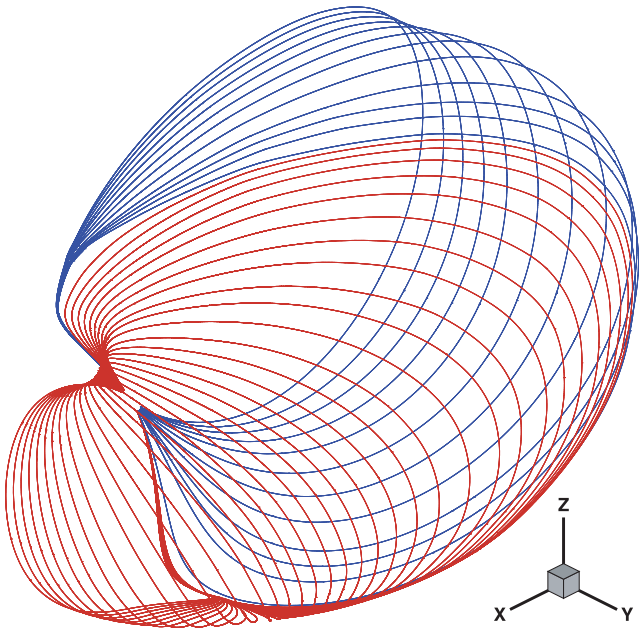

Figure 6. A three-dimensional view of the duskside half of the torus. Blue lines represent separatrix α (Figure 4), while red lines represent separatrix β (Figure 5). The blue lines are behind the red lines when they intersect.

and the subregion facing separatrix β (Closed-β). Of course, well inside the torus, there is no definitive boundary between Closed-α and Closed-β. We distinguish the two only when we talk about the vicinity of the torus surface. Next we divide the IMF region into the subregion facing separatrix γ (IMF-γ) and the subregion facing separatrix δ (IMF-δ). Again, well outside the cylinder, there is no definitive boundary between IMF-γ and IMF-δ. We distinguish the two only when we talk about the vicinity of the cylinder surface. Finally, we divide the open region into the subregion between separatrices β and γ (North Lobe) and the subregion between separatrices α and δ (South Lobe). The distinction between North Lobe and South Lobe is straightforward. Field lines in North Lobe are connected to the northern ionosphere, while field lines in South Lobe are connected to the southern ionosphere. Thus there are six topological regions in total bounded by separatrices.

[25] We next consider possible cases of reconnection. At null M, four topological regions (Closed-α, North Lobe, South Lobe, and IMF-γ) meet together. Accordingly, there are six (${}_4C_2$) cases of reconnection associated with null M. We note here that the singular line (stemline) s_1 is shared by Closed-α and North Lobe, and it is the only field line which belongs to Closed-α (or North Lobe) which diverges from null M. It follows that the merging of a Closed-α and a North Lobe field line does not change the geometry of the field lines at all, indicating that this reconnection is topologically insignificant. The situation is the same for the merging of a South Lobe and an IMF-γ field line because the singular line s_3 is the only field line which belongs to South Lobe (or IMF-γ) which diverges from null M. Elimination of the two insignificant cases leaves four cases of topologically possible reconnection associated with null M. Similar reasoning is applied to the reconnection cases associated with null N. At null N, four topological regions (Closed-β, North Lobe, South Lobe, and IMF-δ) meet together. Of the six cases of reconnection, two (merging of a Closed-β and a South Lobe field line which share singular line s_2, and merging of a North Lobe and an IMF-δ field line which share singular line s_4) should be eliminated, leaving four cases of topologically possible reconnection associated with null N. In total, there are eight cases of reconnection that are topologically possible. However, not all of them are physically possible.

[26] Figure 1, introduced in section 1, depicts four types of magnetic reconnection that are physically possible for due northward IMF and significant dipole tilt (boreal summer). As we show below, all four types are occurring in our simulation of the magnetosphere. In Figure 1, field lines are not necessarily in the noon-midnight meridian plane; the nightside field lines in Figure 1c (where point C_3 resides) and in Figure 1d (where point D_3 resides) are on the duskside flank of the magnetosphere. Type A reconnection (Figure 1a) and type C reconnection (Figure 1c) are associated with null M and occur on the magnetopause (magnetopause reconnection), while type B reconnection (Figure 1b) and type D reconnection (Figure 1d) are associated with null N and occur inside the magnetopause (internal reconnection).

[27] Let us overview the four types of reconnection in terms of the null-separator model and the resultant ionospheric convection. Type A reconnection (Figure 1a) is merging of field lines in IMF-γ and Closed-α on the separators near null M. Type B reconnection (Figure 1b) is merging of field lines in North Lobe and South Lobe on the separators near null N. Both type A and type B reconnection drive merging cells in the ionosphere [*Crooker*, 1992]. Type C reconnection (Figure 1c) is merging of field lines in IMF-γ and North Lobe on the separatrix γ surface near null M. This reconnection drives so-called lobe cells in the northern ionosphere [*Crooker*, 1992; *Crooker et al.*, 1998]. Finally, type D reconnection (Figure 1d) is merging of field lines in North Lobe and Closed-β on the separatrix β surface near null N. This reconnection is topologically the same as the internal reconnection for oblique northward IMF proposed by *Tanaka* [1999] and *Watanabe et al.* [2004]. As we discuss below, type D reconnection drives "reciprocal cells" in the southern ionosphere, and at the same time it contributes to the merging cells in the northern ionosphere.

[28] In Figure 1a, points A_1, A_2, A_3, and A_4 indicate plasma particles attached to the reconnecting field lines. Similarly, in Figures 1b, 1c, and 1d, the plasma particles are denoted with symbols B_1 to B_4, C_1 to C_4, and D_1 to D_4, respectively. The topology of the magnetic field line to which a plasma particle is attached changes by reconnection. We can interpret this topology change as a transition of the plasma particle from one topological region to another. For example, plasma particle A_1 crosses separatrix γ during the reconnection to transfer from IMF-γ to North Lobe. In the following, we denote this separatrix crossing of plasma particle A_1 simply as transition A_1. For each type of reconnection, we can identify four kinds of transition, one for each of the four particles marked in Figures 1a, 1b, 1c, and 1d. For type A reconnection, for example, the four transitions are A_1 (IMF-γ to North

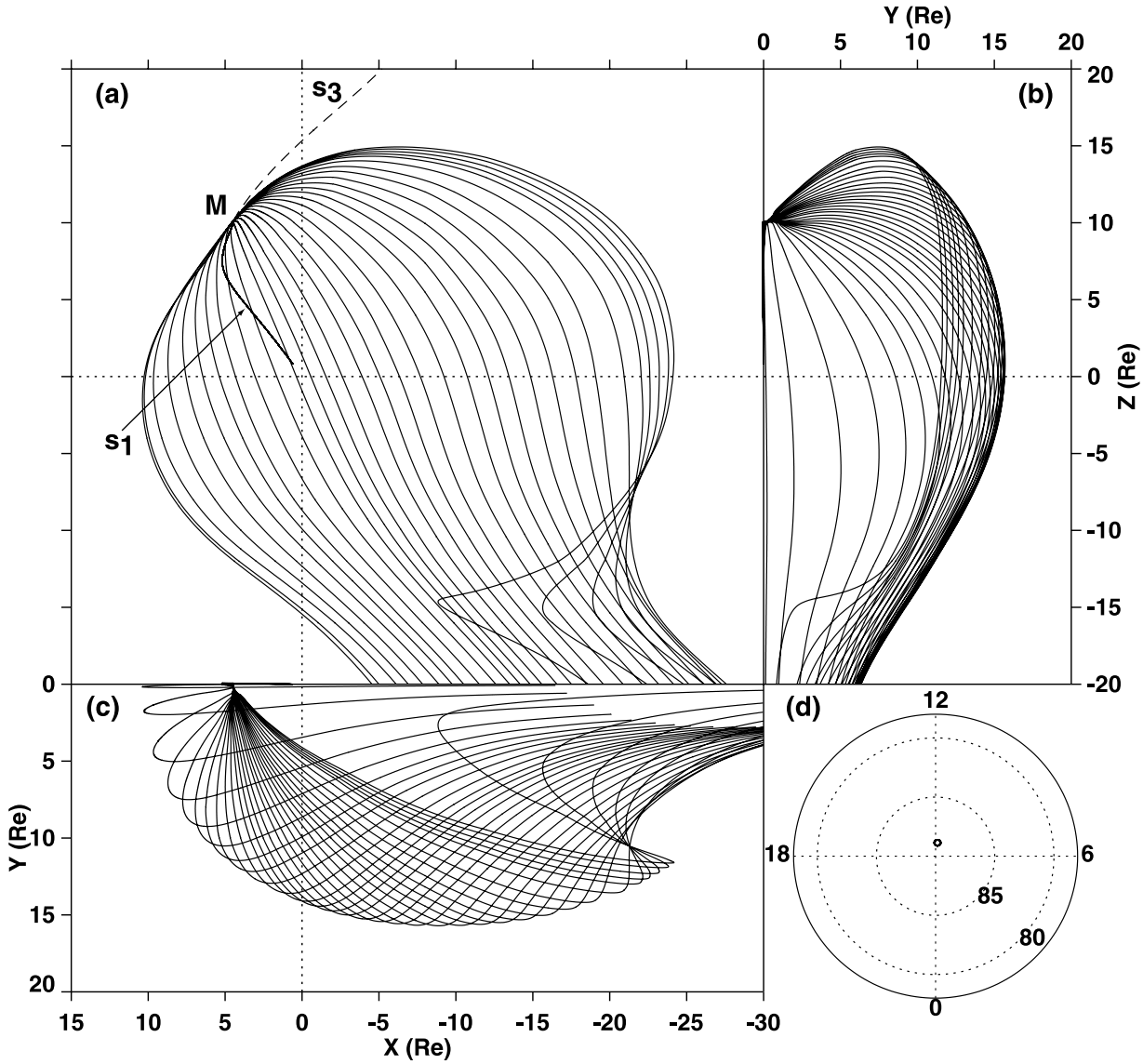

Figure 7. Field lines traced from just inside the duskside open/interplanetary field line boundary at $Z = -30\ R_E$, in the same format as Figure 4. The footpoints of the field lines in the northern ionosphere are shown in Figure 7d by open circles. The dashed line in Figure 7a is a field line when the tracing is started from just outside the open/interplanetary field line boundary at $Z = -30\ R_E$.

Lobe), A_2 (IMF-γ to South Lobe), A_3 (Closed-α to South Lobe), and A_4 (Closed-α to North Lobe).

[29] As listed in Figure 1, there are 16 transitions of plasmas associated with reconnection processes. However, not all of them are unique, and not all of them are observable. Both A_1 and C_1 transitions are from IMF-γ to North Lobe through separatrix γ. Therefore A_1 and C_1 are indistinguishable. Similarly, both B_1 and D_1 transitions are from North Lobe to Closed-β through separatrix β and therefore are indistinguishable. In addition, the topological region to which the plasma particle belongs does not change during the reconnection process in transitions C_2, C_4, D_2, and D_4 (although the geometry of the magnetic field line changes). Therefore these transitions are not observable. Elimination of the indistinguishable and unobservable cases leaves ten plasma transitions across separatrices that can be used to identify the type of reconnection which is occurring.

[30] We now identify the reconnection cases illustrated in Figure 1 in our simulation. Figure 10 shows selected plasma streamlines (white) in the noon-midnight meridian plane, together with cross sections of the four separatrices (pink). Since the system is approximately symmetric with respect to the noon-midnight meridian plane, the streamlines are good approximations of the true streamlines (the Y component of the velocity is very small, and the deviations from the exact symmetry with respect to the $Y = 0$ plane result from the ionospheric Hall conductance [*Ridley et al.*, 2004]). In the noon-midnight meridian plane, the boundaries (s_1) between Closed-α and North Lobe, (s_2) between Closed-β and South Lobe, (s_3) between IMF-γ and South Lobe, and (s_4) between IMF-δ and North Lobe are the four singular field lines converging to or diverging from the two nulls. In the background of Figure 10, plasma pressure is shown for reference. We see that the plasma is flowing across all the

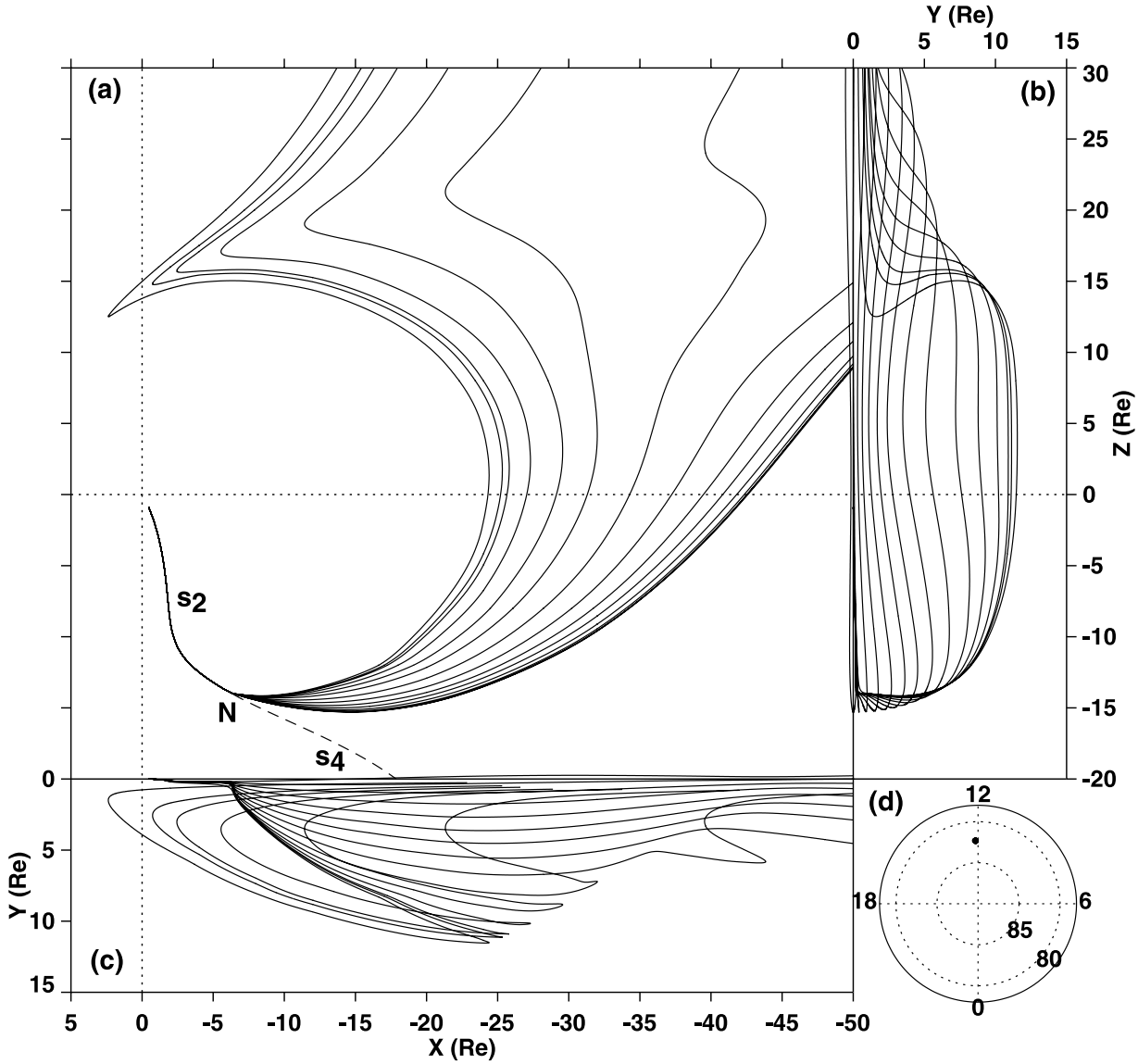

Figure 8. Field lines traced from just inside the duskside open/interplanetary field line boundary at $Z = +30\ R_E$, in the same format as Figure 4. The footpoints of the field lines in the southern ionosphere are shown in Figure 8d by solid circles. The dashed line in Figure 8a is a field line when the tracing is started from just outside the open/interplanetary field line boundary at $Z = +30\ R_E$.

separatrices. Note here that the streamlines near the Earth are nearly field-aligned. These flows are driven by the field-aligned pressure gradient. In our simulation, plasma flow into or out of the inner boundary (a sphere with radius 3 R_E) was allowed because of the zero gradient boundary condition imposed on the velocity component parallel to the magnetic field. Applicability of this boundary condition to the actual magnetosphere-ionosphere system is not entirely known; however, the effect of this boundary condition on the rest of the system is very small.

[31] Figure 11 shows selected two-dimensional streamlines (white) in the equatorial plane (the Z component is not considered), together with four separatrices (pink). For reference, plasma pressure is also plotted in the background. Since the system is not symmetric with respect to the equatorial plane, the streamlines are not the true streamlines. In the subsolar region, the plasma velocity has a significant Z component (Figure 10); therefore the two-dimensional approximation for the streamlines is not valid in the subsolar region of the equatorial plane. Accordingly, streamlines are not plotted in the subsolar region in Figure 11. On the other hand, essential features of the streamlines are not lost in the region plotted in Figure 11. Although the two-dimensional velocity contains a significant field-aligned component (see Figure 10), the streamlines qualitatively represent the cross-field flow responsible for the magnetic flux transport. On the flank and the magnetotail, we can identify plasma flows crossing the separatrices.

[32] Figures 12a and 12b show schematic presentations of Figures 10 and 11, respectively. They illustrate plasma flow (arrows) crossing through separatrices (solid lines) in the noon-midnight meridian plane (Figure 12a) and in the equatorial plane (Figure 12b). Symbols A_1 to A_4, B_1 to B_4, C_1 to C_4, and D_1 to D_4 correspond to those in Figure 1.

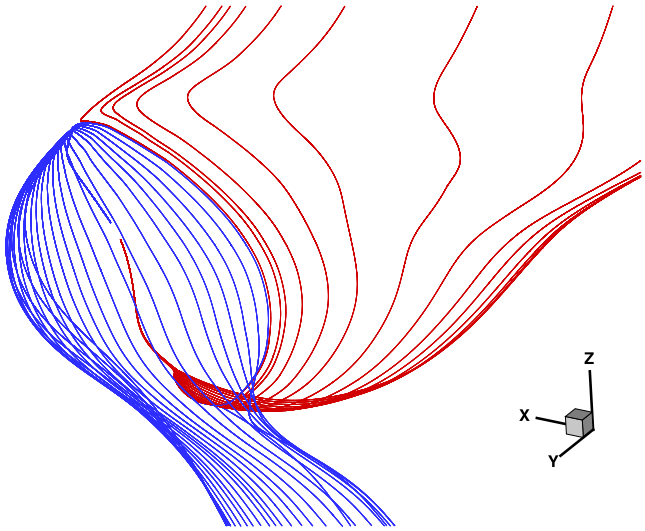

Figure 9. A three-dimensional view of the duskside half of the cylinder. Blue lines represent separatrix γ (Figure 7), while red lines represent separatrix δ (Figure 8). The blue lines are in front of the red lines when they intersect.

Except for C_2, C_4, D_2, and D_4 that are unobservable, all ten of the observable plasma flow crossings in Figure 1 are identified. In particular, C_3 and D_3 are important because they provide unique evidence for type C and type D reconnection processes, respectively. Thus all four types of reconnection shown in Figure 1 are occurring in the simulated magnetosphere.

[33] The reconnection voltage is the electric field integrated along the merging line and is proportional to the total magnetic flux crossing through a separatrix per unit time [*Vasyliunas*, 1984]. The relation between the reconnection voltages of the four types of reconnection is explained using Figure 12b. The geometry of our MHD simulation is almost exactly symmetric with respect to the noon-midnight meridian plane. Therefore we assume that the electric potentials are zero in the $Y = 0$ plane, and we define reconnection voltages (φ) as those associated with duskside ($Y \geq 0$) reconnection. Point T in Figure 12b (open circle) is the equatorial footpoint of the duskside separator. The potential at point T is equal to the reconnection voltage of type A reconnection (φ_A) or type B reconnection (φ_B) (i.e., $\varphi_A = \varphi_B$); as streamlines 1 and 2 in Figure 11 represent, all the streamlines in the equatorial region that pass through separatrix α from Closed-α to South Lobe (A_3) also pass through separatrix δ from South Lobe to IMF-δ (B_3). Note also that the voltages φ_A and φ_B are imposed on the duskside separator, and the net potential drop vanishes along the separator from null N to null M where the potentials are assumed to be zero. On the other hand, points R and U in Figure 12b (open circles) are the potential maxima along separatrices β and γ, respectively, in the equatorial plane. At point R (point U), there is a reversal of plasma flow normal to separatrix β (separatrix γ); plasma is flowing from North Lobe to Closed-β (from IMF-γ to North Lobe) sunward of point R (point U) and from Closed-β to North Lobe (from North Lobe to IMF-γ) tailward of point R (point U). The potential differences between points T and R and between points T and U are equal to the reconnection voltages of type D reconnection (φ_D) and type C reconnection (φ_C), respectively. As streamline 3 in Figure 11 represents, all the streamlines in the equatorial region that cross separatrix β from Closed-β to North Lobe (D_3) also cross separatrix γ from North Lobe to IMF-γ (C_3); however, as streamline 4 represents, there are extra streamlines on the flank that cross separatrix γ but do not cross separatrix β. This imbalance of magnetic flux transport indicates that $\varphi_C > \varphi_D$.

[34] In passing, we mention the cusp-shaped high-pressure region in Figure 10 bounded by separatrix β, separatrix γ, and stemline s_1. The equatorial continuation of this high-pressure region is also seen in Figure 11 (the subsolar orange region bounded by separatrices β and γ). The formation mechanism of this high-pressure region is basically the same as the "cusp" formation mechanism for southward IMF suggested by *Tanaka* [2003, Figure 6]. That is, the Maxwell stress produced by type A and type C reconnection increases the internal energy of the plasma during the southward convection, instead of accelerating the plasma. In fact, the northward part of the high-pressure region is a pumping region ($\mathbf{J} \cdot \mathbf{E} > 0$), while the southward part of the high-pressure region is a dynamo region ($\mathbf{J} \cdot \mathbf{E} < 0$) (where **J** and **E** represent the electric current and the electric field, respectively).

6. Excitation of Lobe Cells and Reciprocal Cells in the Ionosphere (Current Penetration Model)

[35] In the simulated magnetosphere, all the field lines on separatrices converge to or diverge from nulls. If the field lines are equipotentials, the electric field at the ionospheric foot of the stemlines (s_1 and s_2) becomes infinite. This was first suggested by *Stern* [1973] and was called the "Stern singularity" by *Siscoe* [1988], who demonstrated that this problem can be resolved with the addition of a magnetic diffusion region. Within the diffusion region, an electric field parallel to the magnetic field is allowed. In fact, reconnection is a process intrinsically associated with parallel electric fields [e.g., *Vasyliunas*, 1984; *Sonnerup*, 1988]. As discussed in the simulation study by *Crooker et al.* [1998], the result showing that the simulated magnetosphere is approximated by the null-separator model indicates the presence of broad diffusion regions which encompass not only the separators and separatrices but also the neighboring field lines. In the northern (southern) hemisphere, the diffusion region is centered on separatrix γ (separatrix β) and the separators. In general, we expect antiparallel field line geometry outside a diffusion region. For northward IMF, antiparallel configuration occurs only at high latitudes, as sketched in Figure 1 and discussed in section 5. Accordingly, although we cannot exactly determine the extent of the diffusion regions in our MHD model, we conclude they are distributed in the polar regions near the two magnetic nulls.

[36] Thus in an orthodox approach based on the simulation results, the potential pattern in the ionosphere should be explained in terms of parallel electric fields. However, this approach is subject to many difficulties. Above all, we cannot assess parallel electric fields in our simulation model. (Our simulation model assumes ideal MHD, and

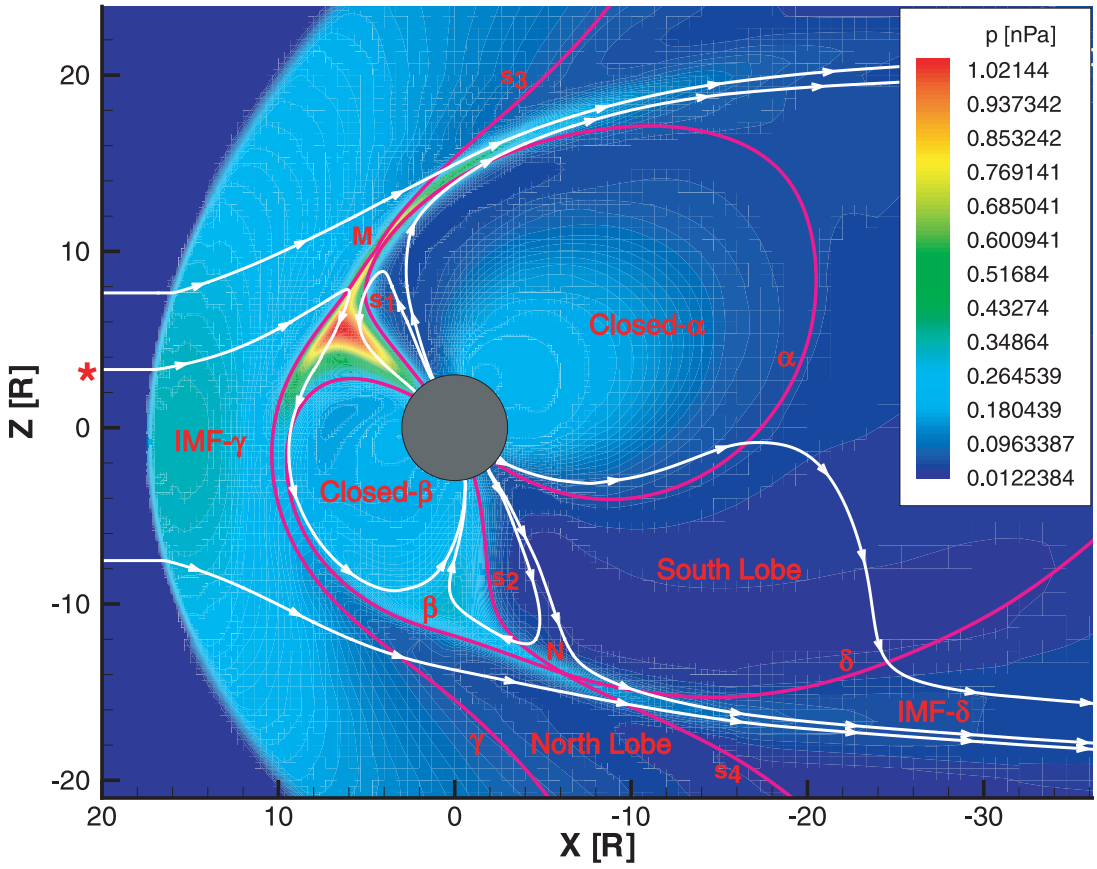

Figure 10. Selected streamlines (white lines with arrows) in the noon-midnight meridian plane ($Y = 0$), together with separatrices (pink). Plasma pressure is shown in the background. Lines s_1, s_2, s_3, and s_4 are the singular field lines diverging from or converging to the two magnetic nulls.

the parallel electric fields arise from numerical diffusion.) In order to circumvent this difficulty, let us consider an alternative approach called the current penetration model by *Siscoe* [1988]. This class of merging models was first proposed by *Alekseyev and Belen'kaya* [1983] and later developed by *Crooker et al.* [1990]. A current penetration model is obtained by adding a normal magnetic field component to the separatrix surface of the vacuum null-separator model. The normal magnetic field is controlled by electric currents confined to an infinitesimally thin layer on the boundary surface. The effect of reconnection is attributed to the boundary currents through which the magnetic field penetrates. The merging line is formed where the normal component of the magnetic field vanishes. In contrast to the null-separator model, the merging line need not be a field line. (In the null-separator model, the merging line is a field line which is on a separatrix or a separator which converges to or diverges from a null). Because of the normal component, the magnetic fields on both sides of the boundary are linked directly without an excursion to a null. Therefore the Stern singularity is removed.

[37] On the one hand, adding a normal field component globally to a separatrix to obtain a current penetration model destroys the null-separator topology. On the other hand, the null-separator topology is stable to magnetic field perturbations and cannot be destroyed easily [*Greene*, 1988]. These paradoxical features are reconciled if one recognizes that the current penetration model with an infinitesimally thin current layer is topologically equivalent to the null-separator model with a finite thickness diffusion region [*Siscoe*, 1988; *Crooker*, 1990; *Crooker et al.*, 1990, 1998]. If the diffusion region in the null-separator model collapses into a surface, the null is confined to the boundary surface and effectively disappears. Conversely, when the boundary current in the current penetration model occupies a finite thickness, the null reappears within the current layer. Thus in global current penetration models, the null-separator topology is hidden in the thin current layer. There is, however, one remark here. The current penetration model is highly flexible so that one can add the normal component of the magnetic field arbitrarily. If the penetration field is confined to a patchy region on the separatrix, reconnection can occur without nulls, as modeled for flux transfer events by *Hesse et al.* [1990]. Otherwise nulls are very stable aspects of magnetic topology [*Greene*, 1988] and cannot be dissociated from merging. One of the advantages of the current penetration model is that field lines can be assumed to be equipotentials. This assumption helps to understand the electromagnetic coupling between the magnetosphere and the ionosphere, so we apply the method of the current penetration model to our simulation results.

[38] The reason why the potential peaks in the northern ionosphere are located poleward of the polar cap boundary is explained as follows using a current penetration model.

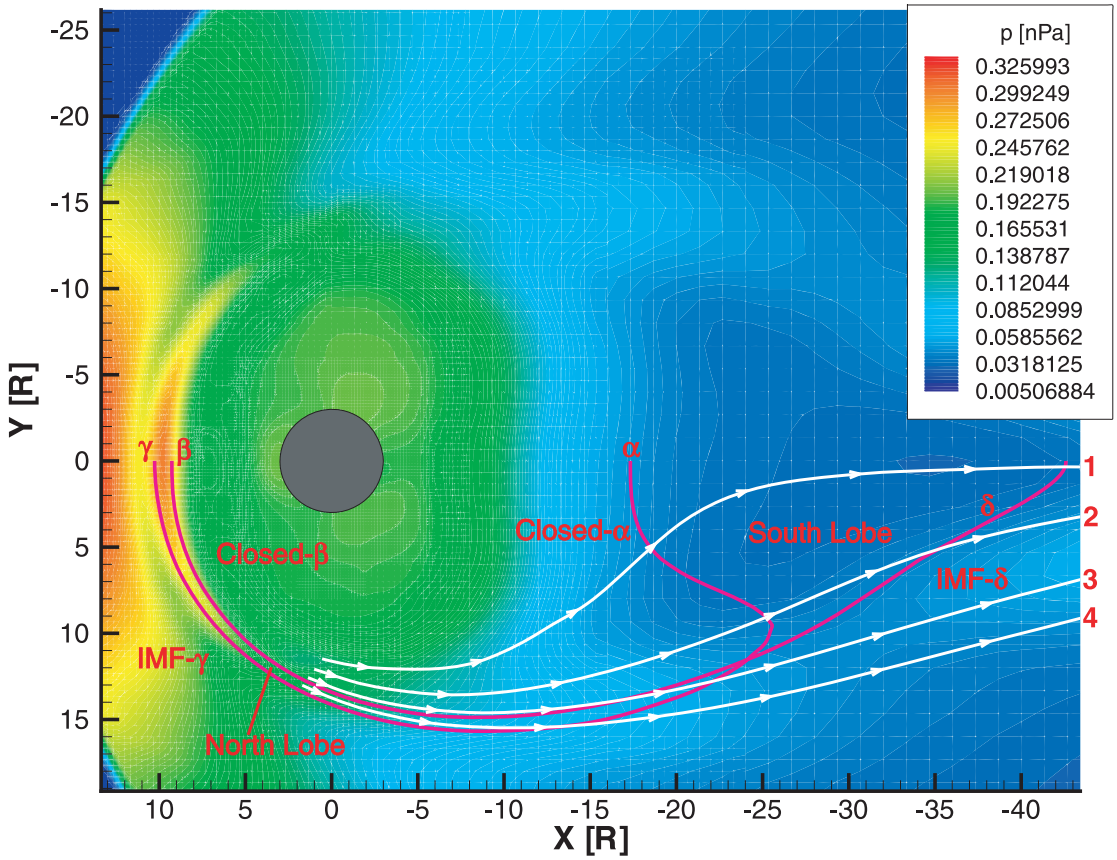

Figure 11. Selected two-dimensional streamlines (white lines with arrows) in the equatorial plane ($Z = 0$), together with separatrices (pink). The Z component of the velocity is not considered. Plasma pressure is shown in the background.

Type C reconnection between IMF-γ and North Lobe field lines occurs on the surface of separatrix γ tailward of null M but sunward of the separators. If the broad diffusion region in the MHD model is confined to a thin current layer on separatrix γ, a normal component of the magnetic field would appear on the boundary. Equivalently, this configuration is obtained by adding, in the vacuum null-separator model, a normal magnetic field component to the separatrix surface corresponding to separatrix γ. Figure 13 shows the current penetration model thus obtained. A thin current layer (diffusion region) has been added only near null M. Field lines C_1 to C_4 correspond to those represented by C_1 to C_4 in Figure 1c, respectively. Outside the diffusion region, field lines C_1 and C_3 run parallel to separatrix γ with an infinitesimally small displacement so that they are virtually on separatrix γ. On the other hand, field lines C_4 (dotted in Figure 13a) are inside the cylinder and go directly into the northern ionosphere without an excursion to null M. (Note that for a field line passing by a null, a small perturbation causes a significant displacement of its ionospheric footpoint.) Therefore the ionospheric projection of the merging line is a line inside the polar cap. Thus the reconnection electric field along the merging line is directly mapped onto the ionosphere, and the peak in the ionospheric potential is shifted poleward of the polar cap boundary. This is the origin of the lobe cells.

[39] Exactly the same reasoning is applied to the formation of reciprocal cells. Type D reconnection between North Lobe and Closed-β field lines occurs on the surface of separatrix β tailward of null N but sunward of the separators. The current penetration model for type D reconnection is obtained by adding, in the vacuum null-separator model, a normal magnetic field component to the separatrix surface corresponding to separatrix β (Figure 14). A thin current layer (diffusion region) has been added only near null N. Field lines D_1 to D_4 correspond to those represented by D_1 to D_4 in Figure 1d, respectively. Outside the diffusion region, field lines D_1 and D_3 are virtually on separatrix β, while field lines D_4 (dotted in Figure 14a) are inside the torus and go directly into the southern ionosphere without an excursion to null N. Therefore the merging line is projected to a line outside the polar cap in the southern ionosphere. Thus the reconnection electric field along the merging line is directly mapped onto the southern ionosphere and shifts the peak in the ionospheric potential equatorward of the polar cap boundary. This is the origin of the reciprocal cells. Meanwhile, in the northern ionosphere, the merging line is projected to two segments on the polar cap boundary, one on the back half (along D_3) and the other on the front half (along D_1). Therefore in the northern ionosphere, type D reconnection contributes to the potential drop across the merging cell. For this, the potential drop

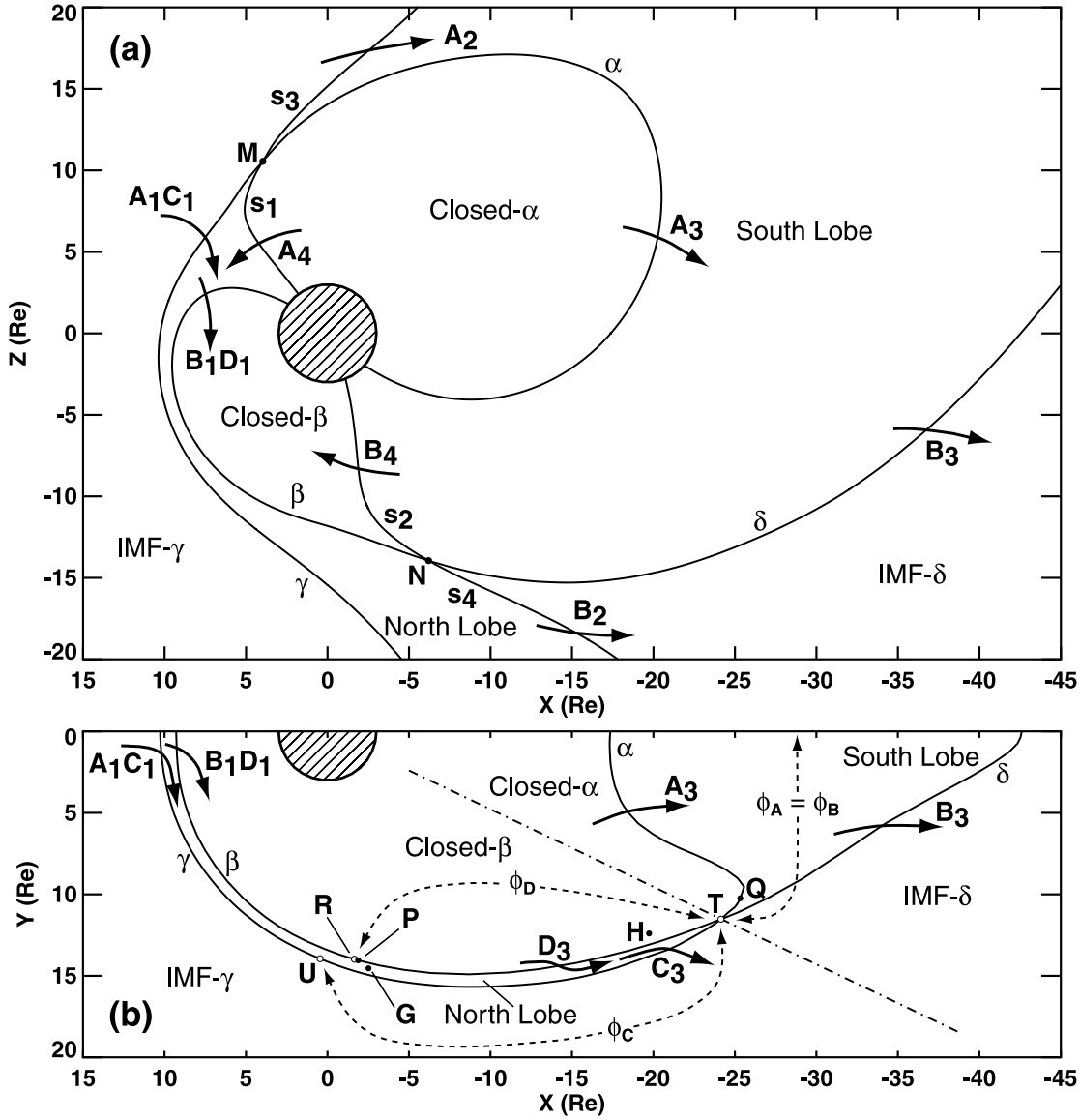

Figure 12. Schematic illustration of plasma transitions (arrows) across separatrices (solid lines) (a) in the noon-midnight meridian plane ($Y = 0$) and (b) in the equatorial plane ($Z = 0$). Symbols A_1 to A_4, B_1 to B_4, C_1 to C_4, and D_1 to D_4 correspond to those in Figure 1. The broken line in Figure 12b indicates the boundaries between Closed-α and Closed-β and between IMF-γ and IMF-δ, but these boundaries have a meaning only in the vicinity of the separatrix surfaces. In Figure 12b, point P (point Q) is the equatorial footpoint of the dropline connecting the northern (southern) ionosphere and null N (null M). Point R (point U) is the reversal of the normal component of the plasma velocity along separatrix β (separatrix γ) in the equatorial plane. Point G (point H) is the equatorial projection of the lobe (reciprocal) cell center in the northern (southern) ionosphere. Dashed arrows denoted with φ_A, φ_B, φ_C, and φ_D represent the reconnection voltages associated with type A, type B, type C, and type D reconnection, respectively.

across the merging cell in the northern ionosphere should be higher than that in the southern ionosphere; however, this is not verified in our simulation.

[40] In the current penetration models in Figures 13 and 14, we considered the current layer only near the magnetic nulls. For type C reconnection in Figure 13b, there is an inward normal component of the magnetic field sunward of the merging line, and in the vicinity of the merging line North Lobe field lines are connected to IMF-γ field lines. We can add this normal component on the entire surface of separatrix γ, as *Crooker* [1992] did in her modeling to make the model magnetopause open (in the sense that the magnetopause is a rotational discontinuity and the lobe field is connected to the IMF). Our MHD simulation also supports this "open" magnetosphere. For type D reconnection in Figure 14b, on the other hand, there is an outward normal component of the magnetic field sunward of the merging line. Unlike type C reconnection, however, we cannot add

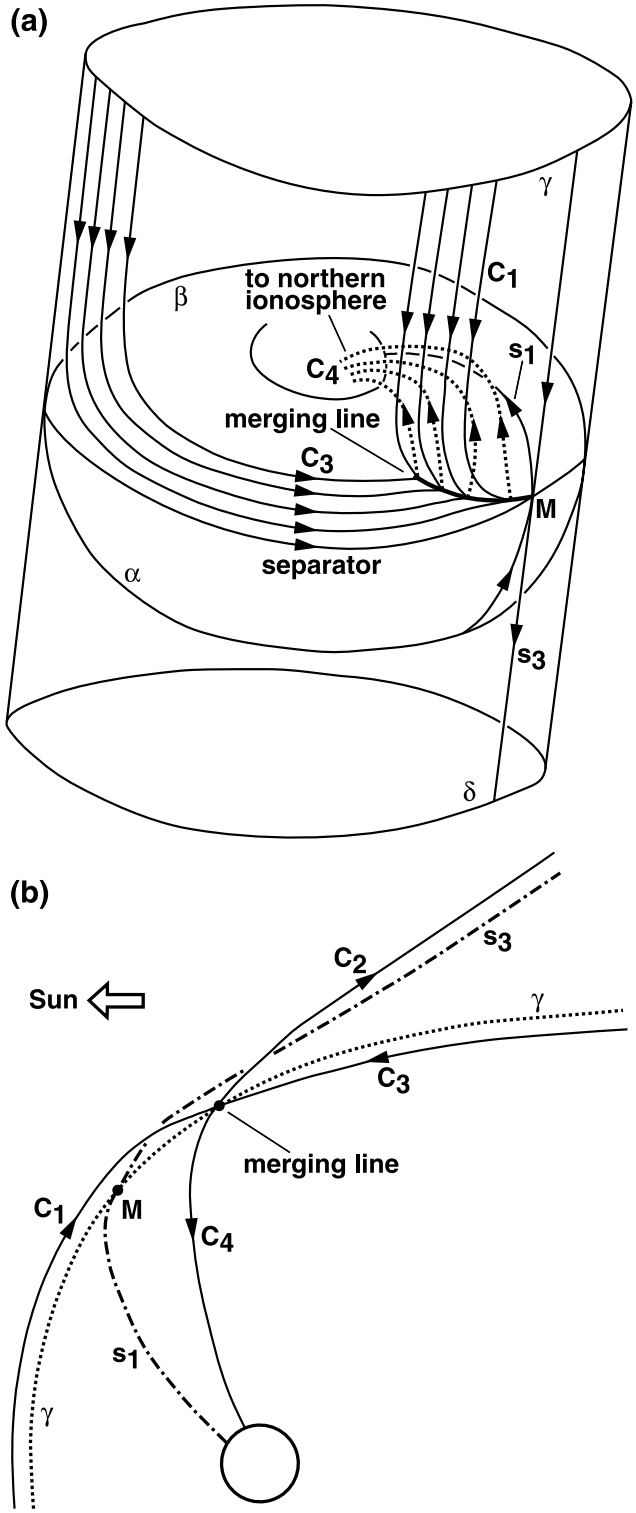

Figure 13. Topology of type C reconnection in the current penetration model: (a) simplified geometry in accordance with Figure 3 and (b) more realistic geometry viewed from the duskside. Field lines C_1 to C_4 correspond to those represented by C_1 to C_4 in Figure 1c, respectively. In Figure 13a, field lines on the cylinder and the torus surface are represented by solid lines, while field lines otherwise are represented by dotted lines. Field lines C_2, which run in the vicinity of singular line s_3, are not shown in Figure 13a for simplicity.

this normal component on the entire surface of separatrix β because the boundary corresponding to separatrix β should be a tangential discontinuity on a global scale.

[41] Figures 13a and 14a also demonstrate how the current penetration model is transformed into the null-

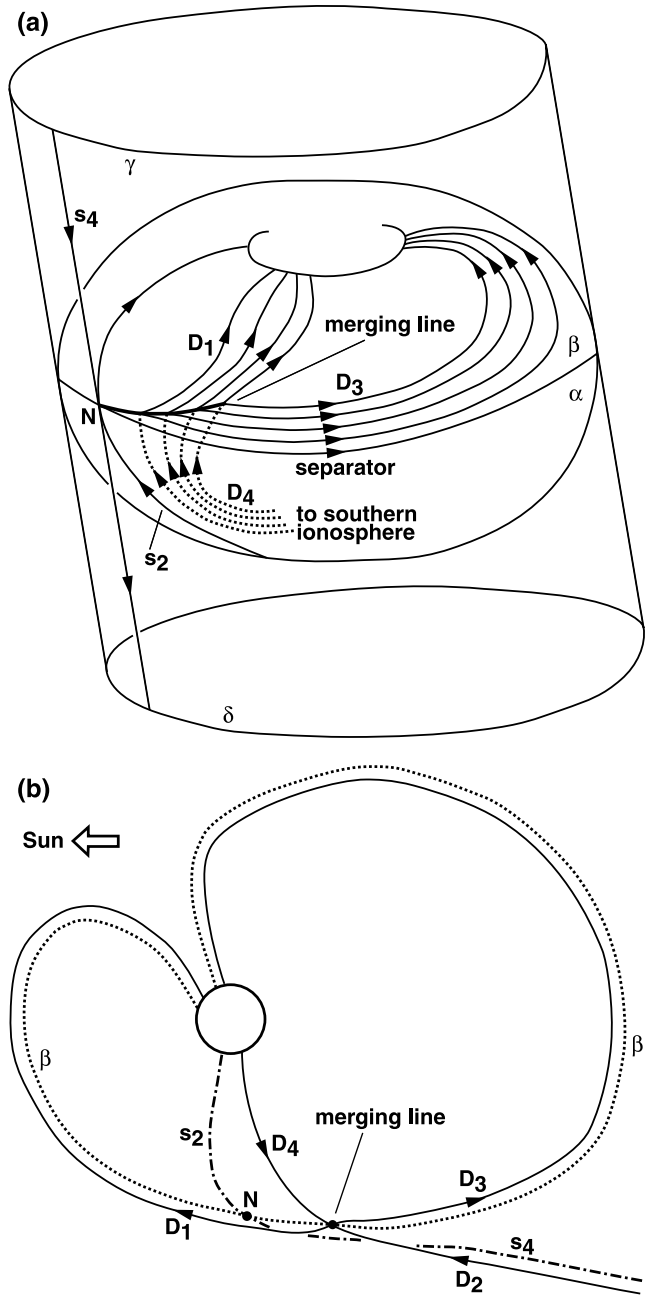

Figure 14. Topology of type D reconnection in the current penetration model: (a) simplified geometry in accordance with Figure 3 and (b) more realistic geometry viewed from the duskside. Field lines D_1 to D_4 correspond to those represented by D_1 to D_4 in Figure 1d, respectively. In Figure 14a, field lines on the cylinder and the torus surface are represented by solid lines, while field lines otherwise are represented by dotted lines. Field lines D_2, which run in the vicinity of singular line s_4, are not shown in Figure 14a for simplicity.

separator model. When the current layer has a finite thickness, the merging line in Figure 13a (Figure 14a) becomes a field line that converges to null M (diverges from null N). Thus the current penetration model is topologically equivalent to the null-separator model.

7. Coupling of Lobe Cells and Reciprocal Cells

[42] Figure 11 indicates that along the streamline labeled 3, transition C_3 occurs after transition D_3 (see also Figure 12b). This means that type C reconnection occurs subsequent to type D reconnection. Also, Figure 10 indicates that along the streamline marked with the asterisk, transition D_1 can occur after transition C_1 (see also Figure 12a). This means that type D reconnection occurs subsequent to type C reconnection. Thus type C and type D reconnection processes are coupled. Let us explain this coupling using Figures 1c and 1d. Type D reconnection is a process that reduces the overdraping of the North Lobe field, while type C reconnection is a process that produces the overdraping of the North Lobe field. In Figure 1d, the overdraped field line (labeled 1) is converted to a relaxed field line (labeled 2) by type D reconnection. Subsequently, the new relaxed field line is included in the process of type C reconnection. Field line 2 in Figure 1d now becomes field line 2 in Figure 1c. In Figure 1c, the relaxed field line (labeled 2) is converted to an overdraped field line (labeled 1) by type C reconnection. This completes one type D to type C cycle, and the next cycle can then begin. Field line 1 in Figure 1c becomes field line 1 in Figure 1d. Thus type C reconnection provides the overdraped field line flux for type D, while type D provides the relaxed field line flux for type C. There is thus a reciprocation of flux between the type C and type D reconnection processes. The nomenclature "reciprocal cells" derives from this reciprocation process.

[43] Let us consider the magnetic flux budget in the reciprocation process. Overdraping of North Lobe field lines is removed not only by type D reconnection but also by type B reconnection. However, since $\varphi_A = \varphi_B$ (section 5), type B reconnection is balanced with type A reconnection that produces overdraping. Therefore the extra amount of overdraping produced by type C reconnection cannot be canceled by type B reconnection. The overdraping produced by type C reconnection is canceled either by type D reconnection or by magnetic flux transport by frozen-in convection. The latter requires motion of North Lobe field lines from the subsolar region to the tail flank of the magnetosphere. Thus the magnetic flux reciprocation between the two reconnection processes indicates that $\varphi_C > \varphi_D$. This is another interpretation of the inequality ($\varphi_C > \varphi_D$) discussed in section 5; in Figure 11, the cancellation of overdraping by frozen-in magnetic flux transport is represented by streamline 4 that experiences transition C_3 but that does not experience transition D_3.

8. Ionospheric Potentials in Terms of the Null-Separator Model: Field-Aligned Potential Drops

[44] In section 6 we interpreted the ionospheric potentials using the current penetration model. However, the ionospheric potentials are actually the consequence of parallel electric fields in the diffusion regions. In the null-separator model, diffusion regions are inevitable to remove the Stern singularity. In this section we interpret the ionospheric potentials in terms of the original null-separator model associated with diffusion regions. Although we cannot quantitatively discuss the potential drop along field lines, a qualitative review is useful for better understanding of the magnetosphere-ionosphere coupling. In the simulated magnetosphere, parallel electric fields are present on the field lines passing through the diffusion regions near the nulls. For both hemispheres, they are directed toward the nulls on the duskside and away from the nulls on the dawnside (roughly in the dusk-to-dawn direction). The diffusion region in the northern (southern) hemisphere is located on the separators and on the adjacent separatrix γ (separatrix β). These diffusion regions have a finite thickness. Note also that along a separator line from null N to null M, the net potential drop vanishes because the potential drops in the two hemispheres cancel each other.

[45] We first consider ionospheric potentials associated with merging cells. As before, we assume that the potentials are zero in the $Y = 0$ plane, where nulls M and N reside. Under this assumption, the ionospheric potentials on the polar cap boundary in Figure 2 represent the potential drop from the corresponding null along the field lines. Of the field lines connecting a null and the ionosphere, the one having the highest (or lowest) potential at the ionospheric foot was called the "dropline" by *Siscoe et al.* [2001]. In our present case, the dropline is the field line giving the largest field-aligned potential drop from the null. The four arrows in Figure 2 indicate the footpoints of droplines. Since the reconnection voltage is proportional to the total magnetic flux crossing a separatrix per unit time [*Vasyliunas*, 1984], the potential at the ionospheric foot of the duskside dropline in the northern (southern) hemisphere should be equal to $\varphi_B + \varphi_D$ (φ_A) (where $\varphi_A = \varphi_B$). Note that the polar cap boundary in the northern (southern) ionosphere is formed by separatrix β (separatrix α). We will examine this prefiguration more in detail.

[46] Point P in Figure 12b (solid circle) is the equatorial footpoint of the duskside dropline connecting the maximum potential on the northern polar cap boundary and null N; point Q is its counterpart for the southern polar cap boundary and null M. Points R and T (open circles) correspond to the potential maxima along separatrices β and α, respectively, in the equatorial plane. As introduced before, point R is the location of reversal of plasma flow normal to separatrix β; point T is the equatorial footpoint of the duskside separator (the edge of separatrix α), and there is no flow reversal along separatrix α in the equatorial plane. We see that points P and R are almost identical, and points Q and T are very close. These indicate that there is little or no potential drop between the northern or southern ionosphere and the equatorial plane along the corresponding droplines. Thus the potential difference of 11.5 kV (10.9 kV) between the northern (southern) ionosphere and null N (null M) comes exclusively from the diffusion region in the southern (northern) hemisphere associated with type B and type D reconnection (type A reconnection). This implies that in our MHD simulation the field lines are equipotentials to a good approximation outside the diffusion regions. There is one important note here. On the one hand, the above discussion indicates that the potential at point R,

for example, is 11.5 kV. On the other hand, we can directly calculate electric potentials in the equatorial plane assuming Ohm's law of ideal MHD. The potential at point R thus directly calculated is much higher than 11.5 kV. From the physical consideration above, we believe that the ionospheric potentials in Figure 2 are undervalued by the simulation code. At the moment, however, the reason for this inconsistency is not known.

[47] Finally, we consider ionospheric potentials associated with lobe cells and reciprocal cells. The potential drops across a lobe cell and a reciprocal cell are related to φ_C and φ_D. Point G in Figure 12b is the equatorial footpoint of the field line giving the maximum potential in the northern ionosphere (i.e., the center of the duskside lobe cell); point H is its counterpart for the southern ionosphere (the field line threading the reciprocal cell center). If the field lines around point G (point H) were equipotentials, a sunward flow would have appeared in the region between point G and separatrix γ (between point H and separatrix β). This convection pattern mismatch indicates the presence of a potential drop between the equator and the northern (southern) ionosphere for field lines threading the region between point G and separatrix γ (between point H and separatrix β). Note also that for the field line threading point U (point R), the potential value of $\varphi_A + \varphi_C$ ($\varphi_B + \varphi_D$) at the equator must become zero at null M (null N). These potential drops occur in the northern (southern) hemisphere diffusion region associated with type A and type C (type B and type D) reconnection. From our present knowledge, we cannot quantify the potentials at the ionospheric foot of these field lines. However, if we adopt the current penetration model in Figures 13 (Figure 14) and assume field lines to be equipotentials, then the maximum potential in the northern (southern) ionosphere is $\varphi_A + \varphi_C$ ($\varphi_B + \varphi_D$). It follows that the potential drop across the lobe (reciprocal) cell in the northern (southern) ionosphere is $\varphi_C - \varphi_D$ (φ_D). (Note again that $\varphi_A = \varphi_B$ and $\varphi_C > \varphi_D$.) The values of φ calculated in the equatorial plane indicate that φ_C is much higher than $2\varphi_D$ (i.e., $\varphi_C - \varphi_D > \varphi_D$). This inequality is reflected on the ionospheric potentials in Figure 2. That is, the potential drops across the lobe cells in the northern ionosphere are larger than those across the reciprocal cells in the southern ionosphere.

9. Relation to the Nontilted Dipole Case

[48] One unique aspect of our MHD simulation is the dipole tilt. So far, several MHD simulations have been performed for due northward IMF, but all of them treated the nontilted dipole case. In terms of the null-separator model, the topology of the magnetosphere becomes singular when the IMF and the dipole axis are parallel. This singularity obscures the basic topology of the magnetosphere. An important example is the work of *Song et al.* [2000], who used a simulation code similar to ours and showed that the "cusp" spreads into an arc in the ionosphere. In light of our simulation results, their arc cusp is considered to be a flattened polar cap. Note also that the "polar cap" boundary by *Song et al.* [2000] is the ionospheric projection of an equatorial boundary dividing the open and the closed streamlines in the equatorial plane and has nothing to do with the polar cap boundary which in this paper is defined topologically to be the open/closed field line boundary. As the dipole tilt decreases, magnetic fluxes in the North Lobe and South Lobe decrease. This means that separatrix β approaches separatrix γ, and separatrix α approaches separatrix δ. In the ionosphere the polar cap shrinks, presumably across the noon-midnight meridian. At the same time, the rates of type C and type D reconnection decrease. In the ionosphere, the potential peaks move to the polar cap boundary, and the lobe cells and the reciprocal cells disappear. When the dipole tilt finally becomes zero, separatrix β and separatrix γ degenerate into a single surface and so do separatrices α and δ. In the ionosphere the polar cap becomes a line with the two potential peaks at its ends. This is the magnetosphere modeled by *Song et al.* [2000], which is a limiting case of the tilted dipole simulation described in the present paper. As suggested by *Greene* [1993], such a magnetospheric configuration is probably unstable as any perturbation to the system will cause the double separatrices to split.

10. Conclusions

[49] Using a numerical MHD simulation, we reexamined *Crooker*'s [1992] magnetosphere model for due northward IMF and significant dipole tilt. We found that the topology of the simulated magnetosphere is well approximated by the null-separator model of *Dungey* [1963] and *Cowley* [1973]. The separatrices and the neighboring field lines are immersed in broad diffusion regions as pointed out by *Crooker et al.* [1998]. We interpreted the ionospheric potentials by applying the method of the current penetration model [*Alekseyev and Belen'kaya*, 1983; *Crooker et al.*, 1990] to our simulation results.

[50] We conclude that internal reconnection occurs not only between a summer lobe and a winter lobe field line, as suggested by *Crooker* [1992], but also between a summer lobe field line and a closed field line. The latter internal reconnection drives "reciprocal cells" that circulate outside the polar cap in the winter ionosphere. We call this reconnection "reciprocal cell reconnection." The reciprocal cells are coupled to the so-called lobe cells that are driven by magnetopause reconnection between an IMF line and a summer lobe field line (lobe cell reconnection); these lobe cells circulate inside the polar cap in the summer ionosphere. The reciprocal cell reconnection converts an overdraped lobe field line to a relaxed lobe field line, while the lobe cell reconnection converts a relaxed lobe field line to an overdraped lobe field line. Thus the role of reciprocal cell reconnection is to reciprocate lobe cell reconnection by canceling the overdraping produced by lobe cell reconnection. In a steady state, from the magnetic flux budget of the overdraped field, the reconnection voltage of reciprocal cell reconnection is smaller than that of lobe cell reconnection. We suggest that in future convection studies, our conclusions above will be verified by the observation of reciprocal cells.

[51] **Acknowledgments.** M. Watanabe was funded by an NSERC (Natural Sciences and Engineering Research Council) Canada CRO (Collaborative Research Opportunities) grant for "Scientific Personnel for the Canadian SuperDARN Program" (G. Sofko, PI). K. Kabin and R. Rankin were supported by NSERC Canada and the Canadian Space Agency. K. Kabin and R. Rankin also acknowledge the use of WestGrid computa-

tional facilities at the University of Alberta. The research at the University of Michigan was supported by DoD MURI grant F49620-01-1-0359, NSF KDI grant ATM-9980078, NSF CISE grant ACI-9876943, NASA ESTO/CT Cooperative Agreement NCC5-614, NASA AISRP grant NAG5-9406, and NSF ITR grant ATM-0325332.

[52] Arthur Richmond thanks Nancy Crooker and John C. Dorelli for their assistance in evaluating this paper.

References

Alekseyev, I. I., and Y. S. Belen'kaya (1983), Electric field in an open model of the magnetosphere, *Geomagn. Aeron.*, *23*, 57–61.

Axford, W. I. (1984), Magnetic field reconnection, in *Magnetic Reconnection in Space and Laboratory Plasmas*, edited by E. W. Hones Jr., pp. 1–8, AGU, Washington, D. C.

Cowley, S. W. H. (1973), A qualitative study of the reconnection between the Earth's magnetic field and an interplanetary field of arbitrary orientation, *Radio Sci.*, *8*, 903–913.

Cowley, S. W. H. (1983), Interpretation of observed relationships between solar wind characteristics and effects at ionospheric altitudes, in *High Latitude Space Plasma Physics*, edited by B. Hultqvist and T. Hagfors, pp. 225–249, Plenum, New York.

Crooker, N. U. (1990), Morphology of magnetic merging at the magnetopause, *J. Atmos. Terr. Phys.*, *52*, 1123–1134.

Crooker, N. U. (1992), Reverse convection, *J. Geophys. Res.*, *97*, 19,363–19,372.

Crooker, N. U., G. L. Siscoe, and F. R. Toffoletto (1990), A tangent subsolar merging line, *J. Geophys. Res.*, *95*, 3787–3793.

Crooker, N. U., J. G. Lyon, and J. A. Fedder (1998), MHD model merging with IMF B_Y: Lobe cells, sunward polar cap convection, and overdraped lobes, *J. Geophys. Res.*, *103*, 9143–9151.

DeZeeuw, D. L., T. I. Gombosi, C. P. T. Groth, K. G. Powell, and Q. F. Stout (2000), An adaptive MHD method for global space weather simulations, *IEEE Trans. Plasma Sci.*, *28*, 1956–1965.

Dungey, J. W. (1963), The structure of the exosphere or adventures in velocity space, in *Geophysics, The Earth's Environment*, edited by C. DeWitt, J. Hieblot, and L. LeBeau, pp. 503–550, Gordon and Breach, New York.

Goodman, M. L. (1995), A three-dimensional, iterative mapping procedure for the implementation of an ionosphere-magnetosphere anisotropic Ohm's law boundary condition in global magnetohydrodynamic simulations, *Ann. Geophys.*, *13*, 843–853.

Greene, J. M. (1988), Geometrical properties of three-dimensional reconnecting magnetic fields with nulls, *J. Geophys. Res.*, *93*, 8583–8590.

Greene, J. M. (1993), Reconnection of vorticity lines and magnetic lines, *Phys. Fluids B*, *5*, 2355–2362.

Hesse, M., J. Birn, and K. Schindler (1990), On the topology of flux transfer events, *J. Geophys. Res.*, *95*, 6549–6560.

Huang, C.-S., G. J. Sofko, A. V. Koustov, D. A. Andre, J. M. Ruohoniemi, R. A. Greenwald, and M. R. Hairston (2000), Evolution of ionospheric multicell convection during northward interplanetary magnetic field with $|B_Z/B_Y| > 1$, *J. Geophys. Res.*, *105*, 27,095–27,107.

Powell, K. G., P. L. Roe, T. J. Linde, T. I. Gombosi, and D. L. DeZeeuw (1999), A solution-adaptive upwind scheme for ideal magnetohydrodynamics, *J. Comp. Phys.*, *154*, 284–309.

Reiff, P. H., and J. L. Burch (1985), B_Y-dependent dayside plasma flow and Birkeland currents in the dayside magnetosphere: 2. A global model for northward and southward IMF, *J. Geophys. Res.*, *90*, 1595–1609.

Ridley, A. J., T. I. Gombosi, and D. L. DeZeeuw (2004), Ionospheric control of the magnetosphere: Conductance, *Ann. Geophys.*, *22*, 567–584.

Siscoe, G. L. (1988), The magnetospheric boundary, in *Physics of Space Plasmas (1987)*, edited by T. Chang, G. B. Crew, and J. R. Jasperse, pp. 3–78, Sci. Publ., Inc., Cambridge, Mass.

Siscoe, G. L., G. M. Erickson, B. U. Ö. Sonnerup, N. C. Maynard, K. D. Siebert, D. R. Weimer, and W. W. White (2001), Global role of $E_{||}$ in magnetopause reconnection: An explicit demonstration, *J. Geophys. Res.*, *106*, 13,015–13,022.

Sonnerup, B. U. Ö. (1988), On the theory of steady state reconnection, *Comput. Phys. Commun.*, *49*, 143–159.

Song, P., T. I. Gombosi, D. L. DeZeeuw, K. G. Powell, and C. P. T. Groth (2000), A model of solar wind–magnetosphere–ionosphere coupling for due northward IMF, *Planet. Space Sci.*, *48*, 29–39.

Stern, D. P. (1973), A study of the electric field in an open magnetospheric model, *J. Geophys. Res.*, *78*, 7292–7305.

Tanaka, T. (1999), Configuration of the magnetosphere-ionosphere convection system under northward IMF conditions with nonzero IMF B_Y, *J. Geophys. Res.*, *104*, 14,683–14,690.

Tanaka, T. (2003), Formation of magnetospheric plasma population regions coupled with the dynamo processes in the convection system, *J. Geophys. Res.*, *108*(A8), 1315, doi:10.1029/2002JA009668.

Vasyliunas, V. M. (1975), Theoretical models of magnetic field line merging, 1, *Rev. Geophys.*, *13*, 303–336.

Vasyliunas, V. M. (1984), Steady state aspects of magnetic field line merging, in *Magnetic Reconnection in Space and Laboratory Plasmas*, edited by E. W. Hones Jr., pp. 25–31, AGU, Washington, D. C.

Watanabe, M., G. J. Sofko, D. A. André, T. Tanaka, and M. R. Hairston (2004), Polar cap bifurcation during steady-state northward interplanetary magnetic field with $|B_Y| \sim B_Z$, *J. Geophys. Res.*, *109*, A01215, doi:10.1029/2003JA009944.

C. R. Clauer, T. I. Gombosi, and A. J. Ridley, Department of Atmospheric Oceanic, and Space Sciences, University of Michigan, Ann Arbor, MI 48109-2143, USA.

K. Kabin and R. Rankin, Department of Physics, University of Alberta, Edmonton, Alberta, T6G 2J1, Canada.

G. J. Sofko and M. Watanabe, Department of Physics and Engineering Physics, University of Saskatchewan, Saskatoon, Saskatchewan, S7N 5E2, Canada. (watanabe@dansas.usask.ca)